ONLINE METHODS AND SUPPLEMENTARY INFORMATION

The loss-of-function PCSK9^{Q152H} variant increases ER chaperones GRP78 and GRP94 and protects against liver injury

Paul F. Lebeau*[1], Hanny Wassef*[2], Jae Hyun Byun[1], Khrystyna Platko[1], Brandon Ason[3], Simon Jackson[3], Joshua Dobroff[4], Susan Shetterly[3], William G. Richards[5], Ali A. Al-Hashimi[1], Kevin Doyoon Won[1], Majambu Mbikay[2], Annik Prat[6], An Tang[7], Guillaume Paré[8], Renata Pasqualini[9], Nabil G. Seidah[6], Wadih Arap[10‡], Michel Chrétien[2‡] and Richard C. Austin[1‡]

Author Affiliations:

[1]Department of Medicine, McMaster University, The Research Institute of St. Joe's and Hamilton Center for Kidney Research, Hamilton, Ontario, Canada.

[2]Laboratory of Functional Endoproteolysis, Clinical Research Institute of Montreal, affiliated with the University of Montreal, Montreal, Quebec, Canada.

[3]Cardiometabolic Disorders Amgen Research, Inc., South San Francisco, CA, USA.

[4]Bristol Myers Squibb., Redwood City, CA, USA.

[5]23andMe., South San Francisco, CA, USA.

[6]Laboratory of Biochemical Neuroendocrinology, Clinical Research Institute of Montreal, affiliated with the University of Montreal, Quebec, Canada.

[7]Department of Radiology at the Centre Hospitalier Universitaire de Montréal, University of Montreal, Montreal, Quebec, Canada.

[8]Population Health Research Institute and the Departments of Medicine, Epidemiology and Pathology, McMaster University, Hamilton, Ontario, Canada.

[9]Division of Cancer Biology, Department of Radiology Oncology, Rutgers New Jersey Medical School and Rutgers Cancer Institute of New Jersey, Newark, United States of America.

[10]Division of Hematology/Oncology, Department of Medicine, Rutgers New Jersey Medical School and Rutgers Cancer Institute of New Jersey, Newark, United States of America.

* Authors contributed equally to this work.

‡To whom correspondence should be addressed: e-mail: austinr@taari.ca; michel.chretien@ircm.qc.ca; wadih.arap@rutgers.edu

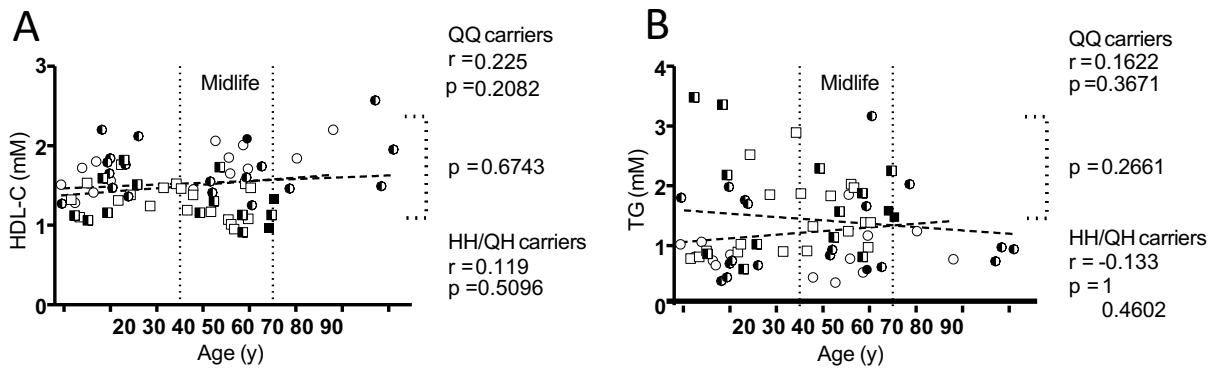

Fig. S1 HDL and triglyceride levels are not altered in PCSK9^{Q152H}-expressing subjects. (A,B) Regression analysis of plasma HDL and triglyceride levels were examined in homozygous (black-filled shapes), heterozygous (white/black-filled shapes) and wild-type family siblings (white-filled shapes). Data were stratified by age. Squares represent men and circles represent women.

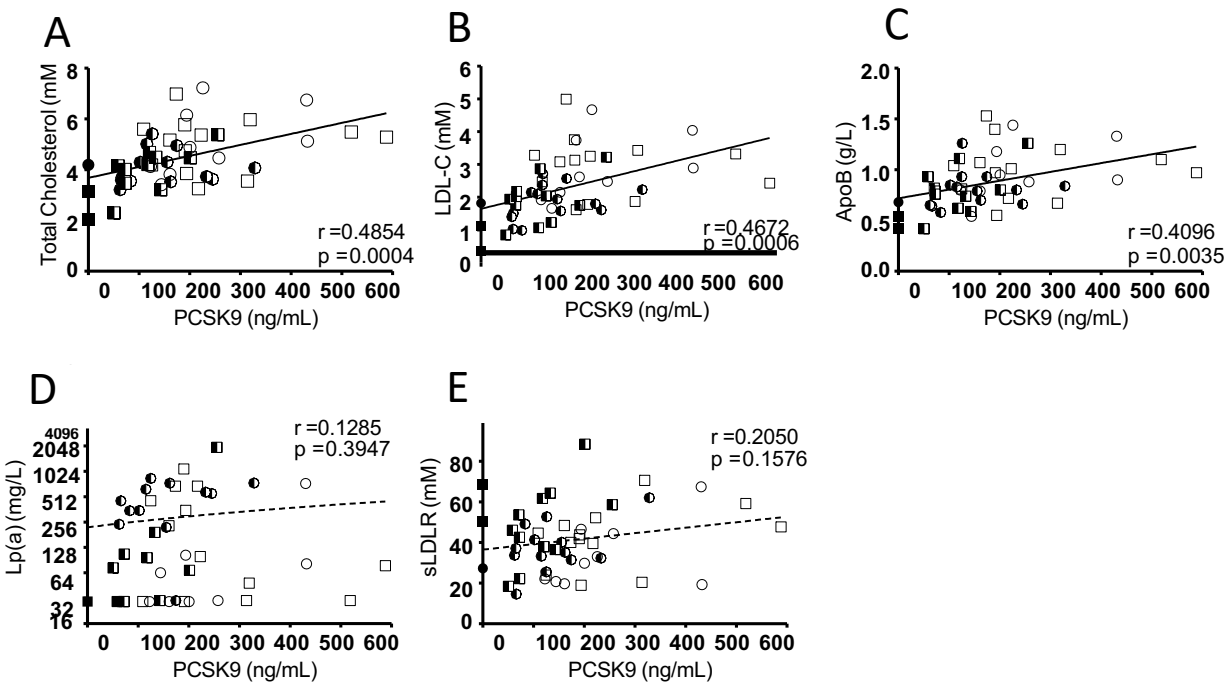

Fig. S2. Total cholesterol, LDLc and ApoB correlate with circulating PCSK9 levels in pooled datasets of carrier and non-carrier family siblings. Regression analysis was carried out to determine the correlation between circulating PCSK9 and (**A**) total cholesterol, (**B**) LDLc, (**C**) ApoB, (**D**) Lp(a) and (**E**) sLDLR. Homozygous carriers are indicated as black-filled shapes, heterozygous carriers as black/white-filled shapes and non-carriers as white-filled shapes. Men are indicated as squares and women as circles.

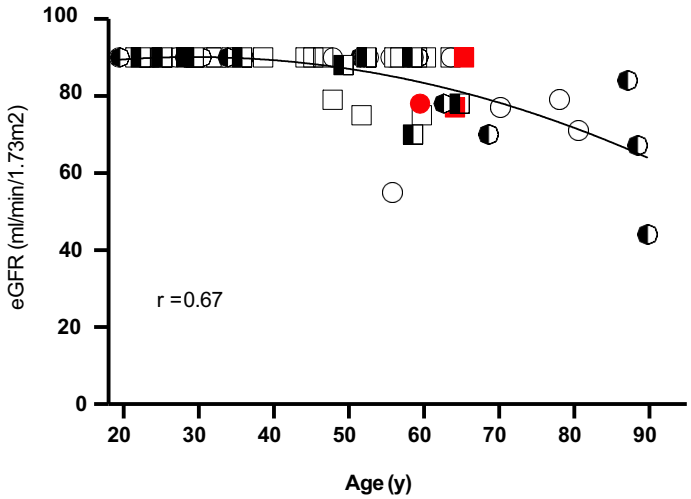

Fig. S3. Carriers of the PCSK9^{Q152H} genetic variation exhibit normal kidney function. Regression analysis was carried out to examine renal function in carriers of the PCSK9^{Q152H} genetic variation. Homozygous carriers are indicated as black-filled shapes, heterozygous carriers as black/white-filled shapes and non-carriers as white-filled shapes. Men are indicated as squares and women as circles.

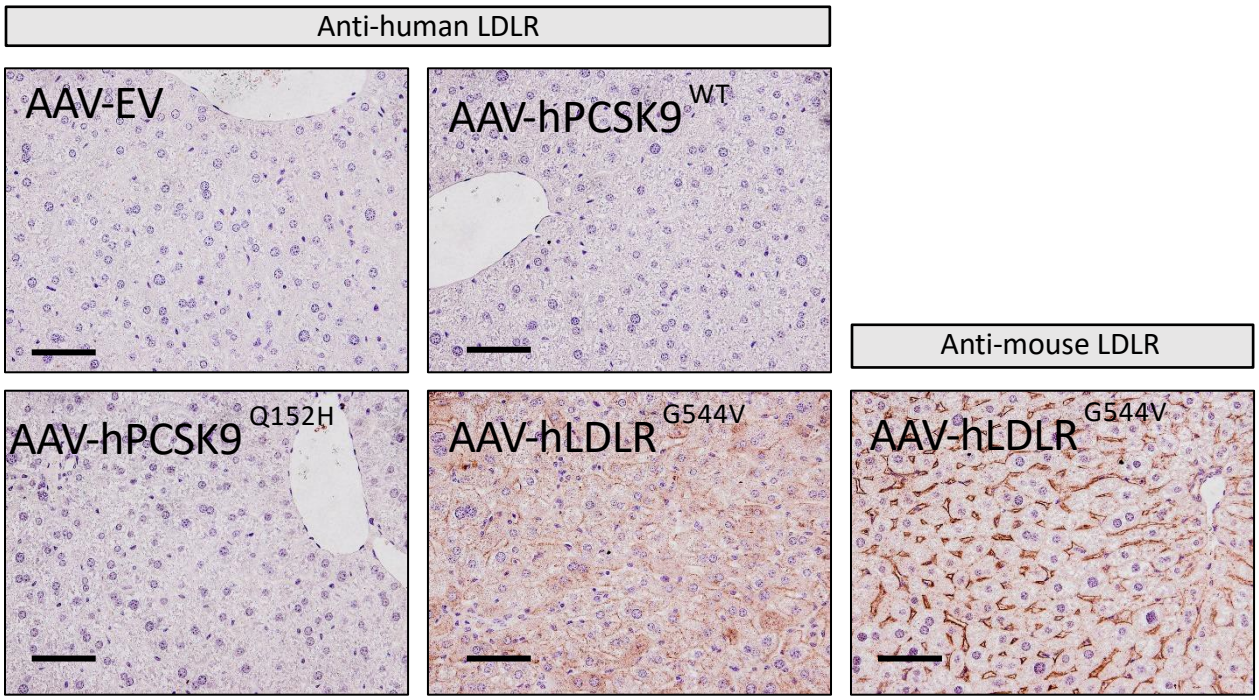

Fig. S4. The G544V mutation causes the accumulation of LDLR in hepatocytes. The expression and cellular localization of the human isoform of AAV-expressed LDLR^{G544V} was examined in the livers of *Pcsk9*$^{-/-}$ mice (n=5) and compared to wild-type mouse LDLR by using two different antibodies targeted against human and mouse LDLR, respectively. Scale bars, 50 µm.

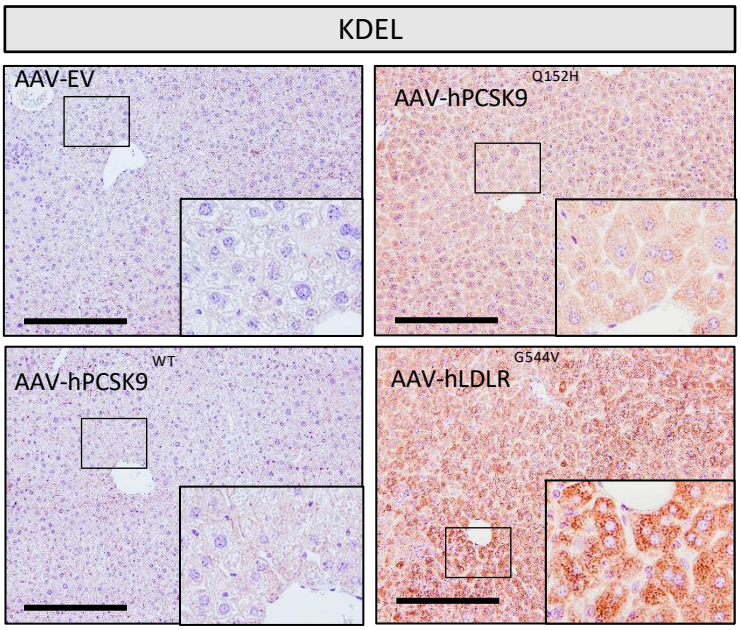

Fig. S5. ER PCSK9 retention increases the abundance of hepatic chaperones containing the KDEL ER-localization peptide. The expression of ER-localized chaperones containing the KDEL sequence was assessed in *Pcsk9*$^{-/-}$ mice (n=5) treated AAVs encoding either empty vector (EV), wild-type (WT) secreted PCSK9 or the ER-retained variants PCSK9^{Q152H} and LDLR^{G544V} via immunohistochemical staining. Values are represented as mean and error bars as S.D. Scale bars, 200 µm.

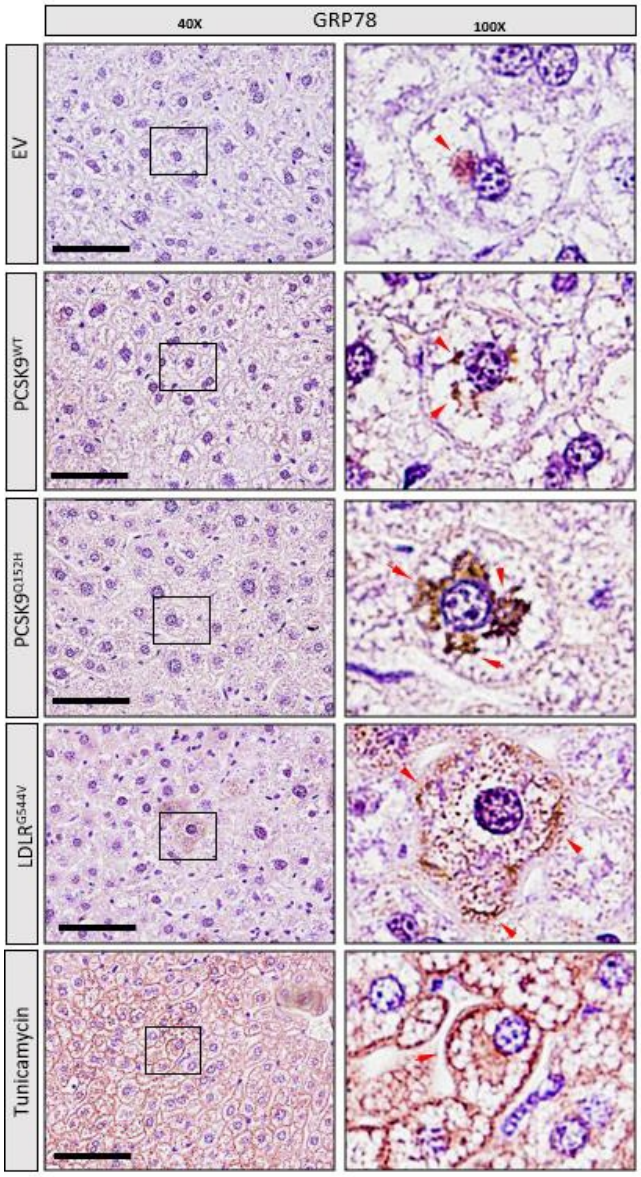

Fig. S6. ER PCSK9 retention induces ER expansion but fails to promote cell-surface localization of GRP78. The livers of *Pcsk9*$^{-/-}$ mice (n=5) treated with AAVs encoding human wild-type PCSK9 (PCSK9^{WT}), as well as two variants that fail to exit the ER, PCSK9^{Q152H} and LDLR^{G544V}, were examined for cellular localization of GRP78 via immunohistochemical staining. The livers of tunicamycin (TM)-treated *Pcsk9*$^{+/+}$ mice served as positive controls for ER stress-induced cell surface localization of GRP78. Scale bars; 50 µm.

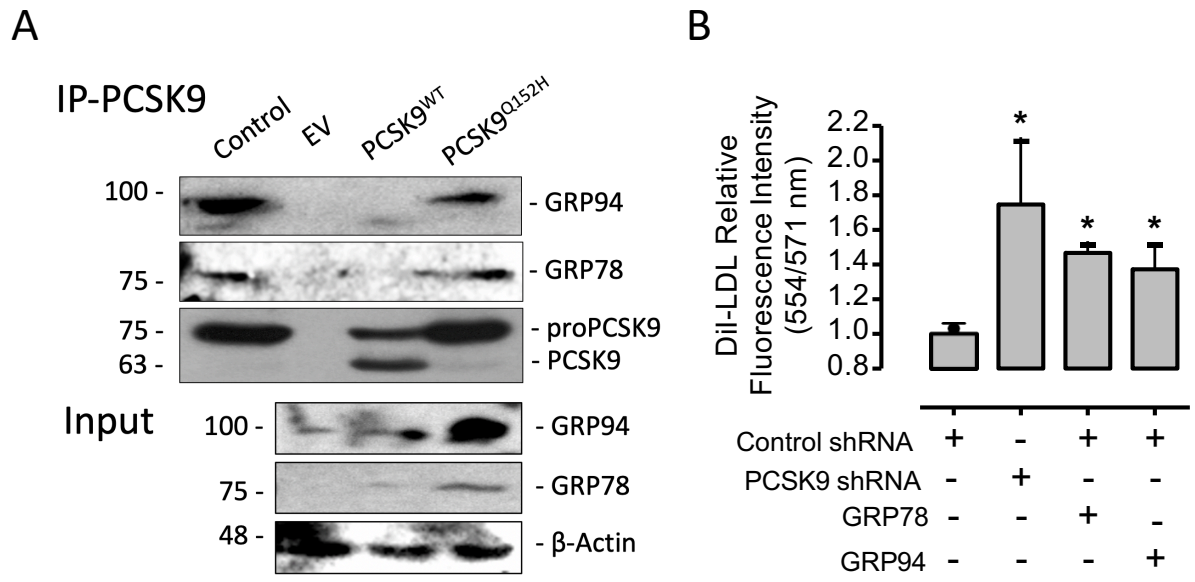

Fig. S7. ER-retained PCSK9 interacts directly with GRP78 and GRP94. (**A**) The interaction between ER-resident PCSK9 and chaperones GRP78 and GRP94 was assessed via immunoprecipitation of human (h)PCSK9 from the livers of mice treated with either AAV-hPCSK9 wild-type (PCSK9WT) or ER-retained variant AAV-hPCSK9Q152H. Additional immunoblots of input lysates for GRP94 and GRP78 confirm the increased abundance of these chaperones in the livers of PCSK9Q152H AAV-treated mice; β-actin serves as a control for immunoblot loading. (B) The interaction between GRP78/GRP94 and PCSK9 was further examined via analysis of LDLR activity; a well-established target of secreted PCSK9 (23). shRNA control or PCSK9 shRNA knockdown HepG2 cells were transfected with mammalian expression vectors encoding either GRP78 or GRP94. The uptake and accumulation of exogenously added fluorescently-labelled DiI-LDL was examined using a fluorescent spectrophotometer (Molecular Devices). Values are represented as mean and error bars as S.D. *, $P < 0.05$ vs. Control shRNA. ANOVA and t test were used for all statistical comparisons.

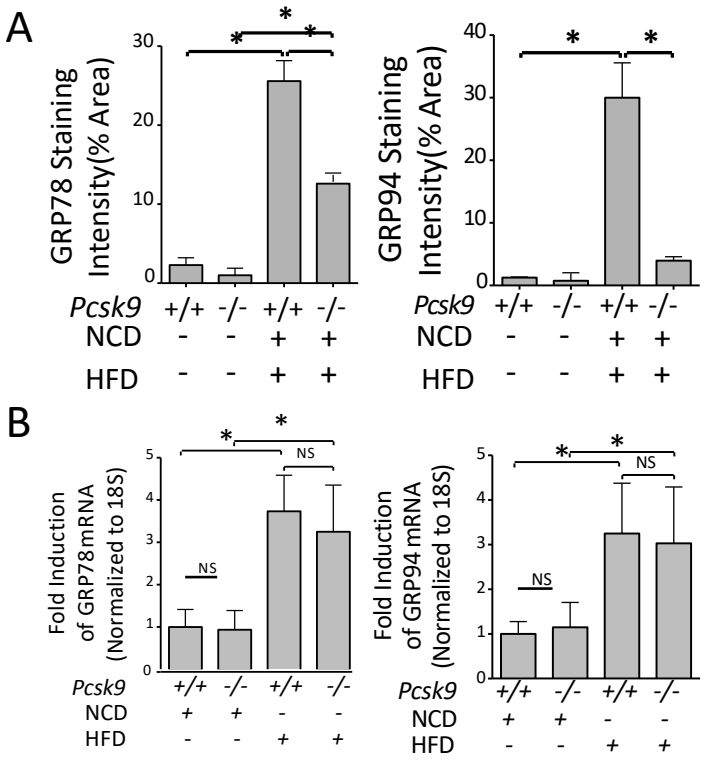

Fig. S8. *Pcsk9*$^{-/-}$ mice exhibit reduced GRP78 and GRP94 expression in response to diet-induced ER stress. (**A**) Hepatic GRP78 and GRP94 protein levels in *Pcsk9*$^{-/-}$ mice and age-matched *Pcsk9*$^{+/+}$ controls fed either high-fat diet (HFD, n=5) or normal chow diet (NCD, n=5) from 6 weeks of age to 18 weeks of age were assessed by immunohistochemical staining and quantified by using ImageJ Software. (**B**) Hepatic GRP78 and GRP94 mRNA expression was also examined via real time PCR. *, $P < 0.05$. ANOVA and *t* test were used for all statistical comparisons.

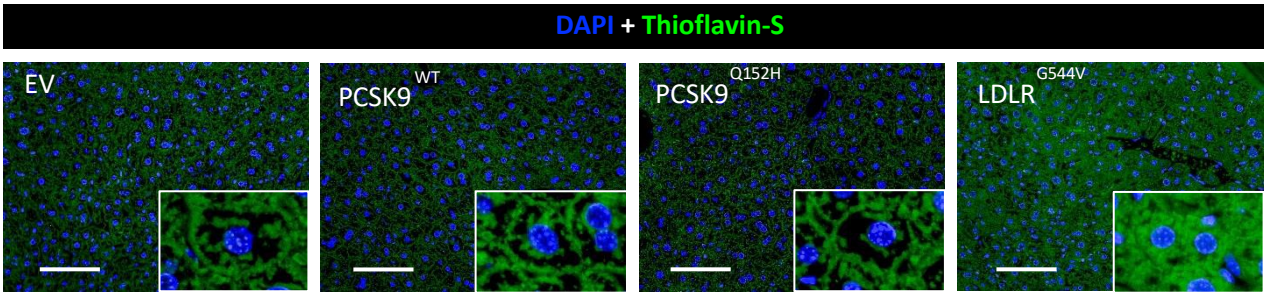

Fig. S9. Hepatic expression of LDLR^{G544V}causes the accumulation of misfolded protein aggregates in the livers of mice. The livers of Pcsk9-/- mice (n=5) treated with adeno-associated virus (AAV) encoding empty vector (EV), human (h)PCSK9 wild-type (WT) and ER-retained variants hPCSK9Q152H and hLDLRG544V were examined for the amyloid accumulation using Thioflavin-S (green). Scale bars, 200 µm.

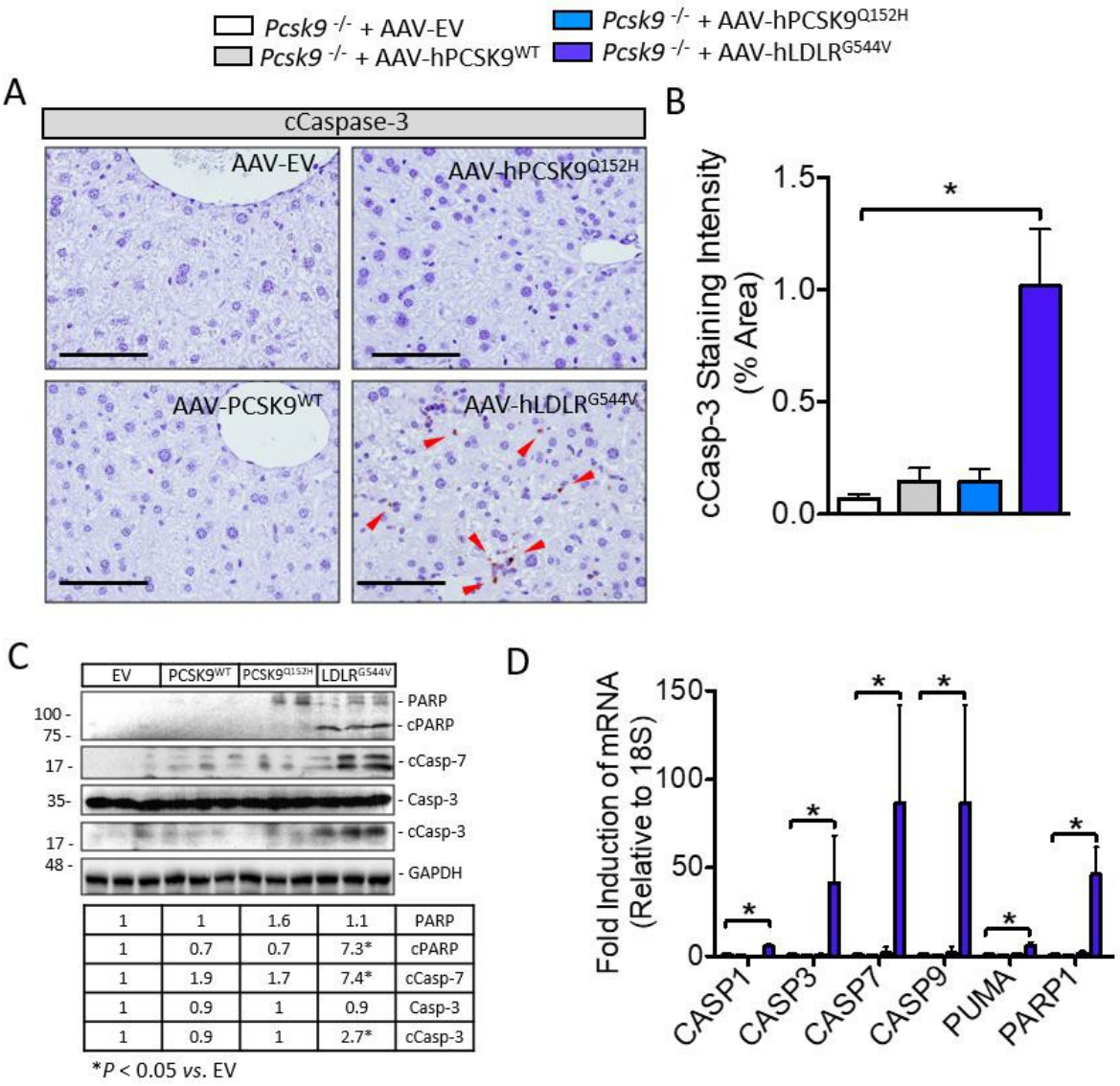

1	1	1.6	1.1	PARP
1	0.7	0.7	7.3*	cPARP
1	1.9	1.7	7.4*	cCasp-7
1	0.9	1	0.9	Casp-3
1	0.9	1	2.7*	cCasp-3

*$P < 0.05$ *vs.* EV

Fig. S10. ER retention of two protein variants, LDLR^{G544V} and PCSK9^{Q152H}, differentially affects apoptosis. (**A,B**) The livers of *Pcsk9*$^{-/-}$ mice (n=5) treated with adeno-associated virus (AAV) encoding empty vector (EV), human (h)PCSK9 wild-type (WT) and ER-retained variants hPCSK9^{Q152H} and hLDLR^{G544V} were examined for expression of cleaved (c)Caspase-3 via immunohistochemical staining, which was quantified using ImageJ software. (**C,D**) Additional pro-apoptotic markers including, PARP, cleaved PARP (cPARP), caspase-1 (CASP1), caspase-3 (CASP3), caspase-7 (CASP7), cleaved caspase-3 (cCasp-3), cleaved caspase-7 (cCasp7) and PUMA were also examined by using immunoblots and real-time PCR. Values are represented as mean and error bars as S.D. *, $P < 0.05$. ANOVA and *t* test were used for all statistical comparisons. Scale bars, 50 µm.

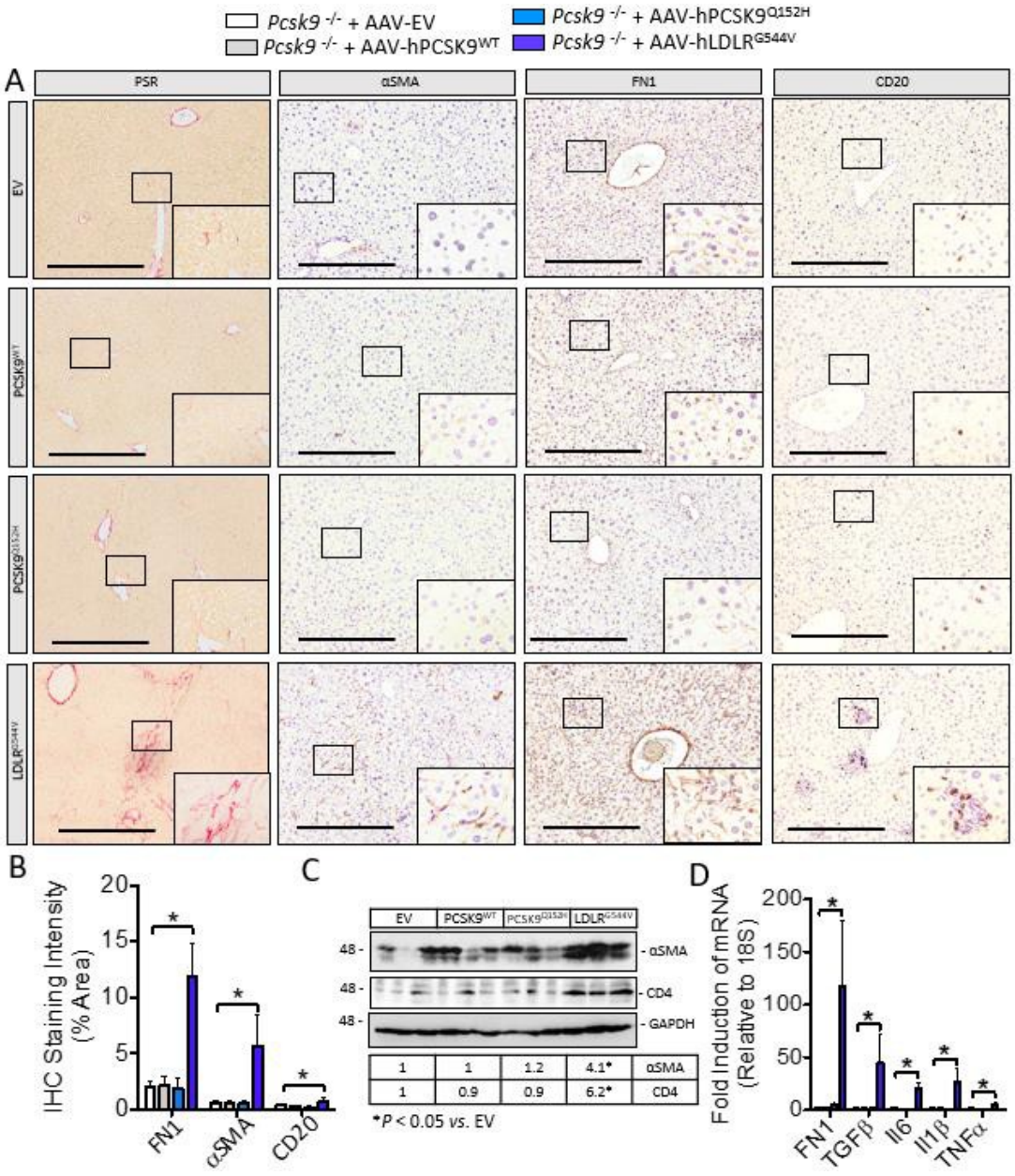

Fig. S11. ER retention of LDLR^{G544V} promotes fibrosis and increases the abundance of CD20-positive inflammatory macrophages. (**A**) The livers of *Pcsk9*$^{-/-}$ mice (n=5) treated with adeno-associated virus (AAV) encoding empty vector (EV), human (h)PCSK9 wild-type (WT) and ER-retained variants hPCSK9^{Q152H} and hLDLR^{G544V} were examined for fibrotic collagen deposition using picrosirius-red (PSR) staining. Immunohistochemical staining was used to assesses hepatic deposition of α-smooth muscle actin (αSMA) and fibronectin (FN1) and infiltration of CD20 positive inflammatory macrophages. (**B**) Staining was quantified using ImageJ software. (**C,D**) Additional pro-fibrotic markers, including αSMA, FN1 and TGFβ, as well as pro-inflammatory markers including CD4, IL6 and IL1β were examined using immunoblots and real-time PCR. Values are represented as mean and error bars as S.D. *, $P < 0.05$ *vs*. EV. ANOVA and *t* test were used for all statistical comparisons. Scale bars, 200 µm.

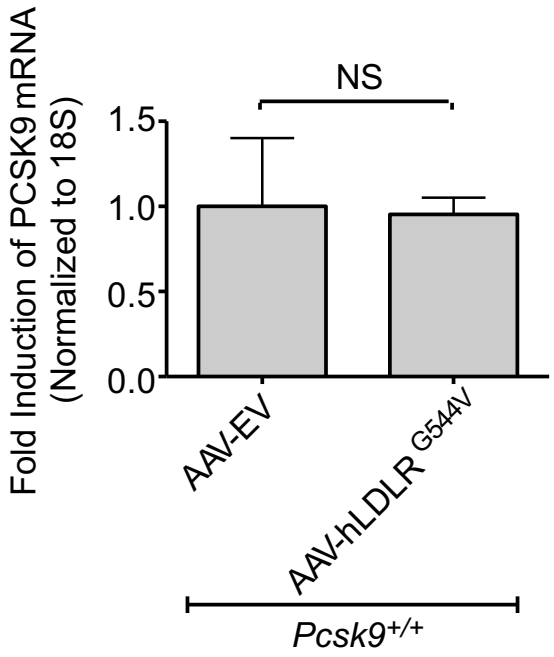

Fig. S12. The expression of hLDLR^{G544V} does not affect de novo PCSK9 expression. PCSK9 mRNA transcript in the livers of mice treated with AAV-EV and AAV-hLDLR^{G544V} was assessed via real-time PCR. Values are expressed as the mean and error bars as SD. *, $P < 0.05$. The *t* test was used for statistical comparison.

Table S1

	A				B				
	HH		QH		HH/QH (average)		QQ		p-value *
	Ave ± SD	N	Ave ± SD	N	Ave ± SD	N	Ave ± SD	N	HH/QH vs QQ
Age (y)	63 ± 3 (59 - 65)	3	47 ± 20 (20 - 91)	30	48 ± 20 (20 - 91)	33	44 ± 16 (19 - 78)	33	0.3660
Sex (M/F)	2/1	3	12/18	30	14/19	33	19/14	33	0.2246
BMI (kg/m^2)	25.9 ± 3.8 (22.8 - 30.2)	3	24.5 ± 3.8 (17.7 - 31.7)	29	24.6 ± 3.9 (17.7 - 31.7)	32	25.6 ± 3.7 (18.4 - 31.9)	30	0.3298
Systolic Pressure (mm Hg)	128 ± 9 (118 - 136)	3	120 ± 15 (91 - 140)	29	121 ± 14 (91 - 140)	32	121 ± 14 (95 - 148)	28	0.9053
Diastolic Pressure (mm Hg)	77 ± 5 (72 - 82)	3	76 ± 9 (56 - 94)	29	76 ± 9 (56 - 94)	32	75 ± 8 (58 - 89)	28	0.8099
PCSK9 (ng/ml)	0 ± 0 0	3	134 ± 72 (50.5 - 328.0)	25	119 ± 80 (0 - 328)	28	250 ± 132 (109.3 - 587.8)	22	0.0001
Total cholesterol (mM)	3.12 ± 1.08 (2.04 - 4.19)	3	4.09 ± 0.67 (2.30 - 5.41)	30	4.00 ± 0.75 (2.04 - 5.41)	33	4.94 ± 1.15 (3.25 - 7.22)	33	0.0002
HDL (mM)	1.46 ± 0.57 (0.97 - 2.09)	3	1.54 ± 0.38 (0.91 - 2.57)	30	1.53 ± 0.39 (0.91 - 2.57)	33	1.48 ± 0.31 (0.95 - 2.20)	33	0.5967
LDL (mM)	1.09 ± 0.74 (0.35 - 1.82)	3	1.89 ± 0.57 (0.85 - 3.22)	30	1.81 ± 0.62 (0.35 - 3.22)	33	2.91 ± 1.00 (1.51 - 4.99)	33	1.00E-06
Non-HDL (mM)	1.65 ± 0.53 (1.07 - 2.1)	3	2.51 ± 0.64 (1.24 - 4.25)	30	2.43 ± 0.67 (1.07 - 4.25)	33	3.46 ± 1.10 (1.82 - 5.60)	33	2.00E-05
ApoB (g/l)	0.55 ± 0.13 (0.42 - 0.68)	3	0.81 ± 0.20 (0.42 - 1.26)	29	0.78 ± 0.20 (0.42 - 1.26)	32	0.96 ± 0.26 (0.54 - 1.53)	30	0.0039
ApoE (ug/ml)	113 ± 6 (106 - 118)	3	139 ± 34 (88 - 231)	24	136 ± 33 (88 - 231)	27	169 ± 38 (94 - 240)	22	0.0026
Triglycerides (mM)	1.22 ± 0.54 (0.60 - 1.58)	3	1.45 ± 0.86 (0.41 - 3.48)	30	1.43 ± 0.83 (0.41 - 3.48)	33	1.21 ± 0.59 (0.38 - 2.89)	33	0.2117
Glucose (mM)	5.73 ± 0.32 (5.5 - 6.1)	3	5.12 ± 0.54 (4.1 - 6.1)	29	5.18 ± 0.55 (4.1 - 6.1)	32	5.13 ± 0.50 (4.4 - 6.6)	29	0.7619
HbA1c (%)	5.47 ± 0.38 (5.2 - 5.9)	3	5.38 ± 0.40 (4.8 - 6.3)	27	5.39 ± 0.39 (4.8 - 6.3)	30	5.31 ± 0.38 (4.4 - 5.9)	29	0.4314
Insulin (pM)	134 ± 95 (77 - 244)	3	60 ± 30 (29 - 172)	29	67 ± 43 (29 - 244)	32	46 ± 17 (14 - 85)	27	0.0182
HOMA	5.8 ± 4.5 (3.1 - 11)	3	2.3 ± 1.2 (1.1 - 7.4)	29	2.6 ± 1.9 (1.1 - 11)	32	1.7 ± 0.6 (0.5 - 2.9)	27	0.0235
Lp(a) (mg/l)	29 ± 0 (29 -29)	3	379 ± 426 (29 - 1981)	26	343 ± 417 (29 - 1981)	29	293 ± 389 (29 - 1497)	28	0.6464
sLDLR (ng/ml)	49 ± 21 (27 - 69)	3	42 ± 17 (15 - 88)	24	43 ± 17 (15 - 88)	27	39 ± 16 (19 - 71)	22	0.3625
TSH (mIU/l)	2.82 ± 2.24 (0.79 - 5.22)	3	2.27 ± 1.56 (0.21 - 7.58)	26	2.33 ± 1.60 (0.21 - 7.58)	29	2.00 ± 1.45 (0.74 - 7.31)	27	0.4171
LDH (U/l)	104.0 ± 45.4 (72 - 156)	3	156.8 ± 30.8 (86 - 207)	25	151.1 ± 35.7 (72 - 207)	28	156.1 ± 25.6 (81 - 207)	28	0.5546
AST (U/l)	21.3 ± 3.5 (18 - 25)	3	20.4 ± 5.5 (13 - 34)	27	20.5 ± 5.3 (13 - 34)	30	22.4 ± 6.9 (13 - 48)	31	0.2137
ALT (U/l)	20.3 ± 6.4 (13 - 24)	3	20.4 ± 12.9 (9 - 60)	28	20.4 ± 12.4 (9 - 60)	31	20.9 ± 10.0 (8 - 47)	31	0.4513
GGT (U/l)	25.3 ± 8.7 (18 - 35)	3	24.0 ± 13.4 (7 - 56)	27	24.1 ± 12.9 (7 - 56)	30	22.2 ± 12.3 (10 - 61)	30	0.4334
Bilirubin (uM)	9.7 ± 2.3 (7 - 11)	3	10.1 ± 3.9 (4 - 22)	27	43.4 ± 2.3 (4 - 22)	30	44.1 ± 2.6 (6 - 38)	29	0.0945
Statin Users	0	3	1	31	1	34	5	38	0.1213
Non-Statin Participants					**33**		**33**		

Table S1. Blood chemistry in healthy volunteers carrying the LOF PCSK9^{Q152H} mutation. Seventy-two subjects underwent complete anthropometry and blood chemistry. Six were excluded from statistical analysis because they were taking statins. (**A**) Except for the absence of detectable plasma PCSK9 in the homozygote carriers, the blood chemistry of homozygous carriers was similar to that of heterozygous carriers. (**B**) All Q152H carriers were pooled together and compared with non-carrier family members. The two genotypic cohorts had similar distributions of age, sex, BMI and blood pressure. HH denotes homozygous carriers, QH denotes heterozygous carriers and QQ denotes non-carriers.

Tables S2 to S8

Table S2. Immunoblot quantification for figure 3F.

EV	PCSK9^{WT}	PCSK9^{Q152H}	LDLR^{G544V}	
1	0.1*	1	1	LDLR-m
1	1	1	4.7*	LDLR-i
1	4.5*	22.5*†	1	proPCSK9
1	7.4*	2.1*†	1	PCSK9

*$P < 0.05$ *vs*. EV; †$P < 0.05$ *vs*. PCSK9^{WT}

Table S3. Immunoblot quantification for figure 4C.

EV	PCSK9^{WT}	PCSK9^{Q152H}	LDLR^{G544V}	
1	1.1	6.2*†	2.8*	GRP94
1	1.1	4.6*†	2.4*	GRP78

*$P < 0.05$ *vs*. EV; †$P < 0.05$ *vs*. LDLR^{G544V}

Table S4. Immunoblot quantification for figure 4F.

Pcsk9$^{+/+}$	*Pcsk9*$^{-/-}$	*Pcsk9*$^{+/+}$	*Pcsk9*$^{-/-}$	
NCD		HFD		
1	0.4*	3.1*	1.5†	GRP94
1	1.2	2.5*	1.1†	GRP78

*$P < 0.05$ *vs*. *Pcsk9*$^{+/+}$ NCD; †$P < 0.05$ *vs*. *PCSK9*$^{+/+}$ HFD

Table S5. Immunoblot quantification for figure 5B.

PCSK9^{WT}	+	-	+	-
PCSK9^{Q152H}	-	+	-	+
TG	-	-	+	+

1	1.1	1.6*	0.5†	pPERK
1	1	2*	1.5†	IRE1α
1	2.1*	3.3*	4.2†	GRP94
1	1.6*	1.9*	2.5†	proPCSK9
1	0.3*	1	0.3†	PCSK9

*$P < 0.05$ *vs*. untreated PCSK9^{WT}
†$P < 0.05$ *vs*. TG-treated PCSK9^{WT}

Table S6. Immunoblot quantification for figure 6A.

EV	PCSK9^{WT}	PCSK9^{Q152H}	LDLR^{G544V}	
1	0.9	0.9	1.9*	pPERK
1	0.9	1.2	6.3*	IRE1α
1	0.9	1.2	1.7*	sXBP1
1	0.9	1	2.3*	peIF2α
1	0.9	1	0.9	eIF2α
1	0.9	1.1	3.5*	CHOP

*$P < 0.05$ *vs*. EV

Table S7. Immunoblot quantification for figure 7C.

AAV-hLDLR^{G544V}		
Pcsk9$^{-/-}$	*Pcsk9*$^{+/+}$	
1	0.6*	IRE1α
1	0.9	XBP1
1	0.5*	sXBP1
1	0.5*	ATF4
1	0.6*	peIF2α
1	0.9	eIF2α
1	1	Casp3
1	0.2*	cCasp3

*, $P < 0.05$ *vs*. *Pcsk9*$^{-/-}$ AAV-hLDLR^{G544V}

Table S8. Immunoblot quantification for figure 7E.

	Dose				
EV	x2	x1	x1	-	
hPCSK9^{Q152H}	-	x1	-	x1	
hLDLR^{G544V}	-	-	x1	x1	
	1	0.7	3.5*	0.8†	pIRE1α
	1	0.8	3.4*	1.8†	ATF6
	1	5.4	4.0*	3.0†	GRP94
	1	2.8	2.7*	1.4†	GRP78
	0	1*	0	1*	proPCSK9
	1	0.87	3.6*	1.6†	sXBP1

*, $P < 0.05$ *vs*. AAV-EV

†$P < 0.05$ *vs*. LDLR^{G544V}

Table S9. List of antibodies and conditions used in the study

Antibody	Catalog no.	Application	Dilution and Protocol
ATF4	D4B8, Cell Signaling	IB	1:1000
CASP3	Ab136812, Abcam	IB	1:500
CASP3	Ab136712, Abcam	IHC	1:500, HIER
CASP7	9491, Cell Signaling	IB	1:500
cPARP	Ab136812, Abcam	IB	1:500
CD20	SC-7733, Santa Cruz Biotechnology	IHC	1:50, HIER
CD4	Sc-19641, Santa Cruz Biotechnology	IB	1:500
eIF2α	SC-133132, Santa Cruz	IB	1:1000
FN1	Biotechnology F3648, Sigma-Aldrich	IHC	1:200, HIER
GAPDH	2118, Cell Signaling	IB	1:1000
GFP-VP	NB600-308, Novus Biologicals	IB	1:1000
GRP78	610979, BD Biosciences	IB	1:1000
GRP78	SC-1050, Santa Cruz Biotechnology	IHC	1:40, no
GRP94	ADI-SPA-850, Enzo Life Sciences ADI-	IHC	retrieval
GRP94	SPA-850, Enzo Life Sciences 3294,	IB	1:100, HIER
IRE1α	Cell Signaling	IB	1:1000 1:1000
KDEL	ADI-SPA-827-D, Enzo Life Sciences	IHC	1:100, HIER
LDLR (mouse)	AF2255, R and D Systems	IHC	1:100, HIER
LDLR (human)	AF2148, R and D Systems	IHC	1:100, HIER
LDLR (immature)	SC-373830, Santa Cruz Biotechnology	IB	1:500
LDLR (mouse)	AF2255, R and D Systems	IB	1:1000
PCSK9	NB300-959, Novus Biologicals	IF	1:100
PCSK9	NB300-959, Novus Biologicals	IB	1:500
PCSK9	NB300-959, Novus Biologicals	IHC	1:500, HIER
peIF2α	3398, Cell Signaling	IB	1:1000
pIRE1α	Ab48187, Abcam	IHC	1:100, HIER
pPERK	3179, Cell Signaling	IB	1:1000
pPERK	Ab192591, Abcam	IHC	1:100, HIER
XBP1	Sc-8015, Santa Cruz Biotechnology	IB	1:1000
αSMA	MA5-11547, ThermoFisher Scientific	IB	1:1000
αSMA	MA5-11547, ThermoFisher Scientific	IHC	1:100, HIER

β-Actin	MA5-15739, ThermoFisher Scientific	IB	1:5000

IB, Immunoblot; IHC, immunohistochemistry; IF, immunofluorescence; HIER, heat-induced epitope retrieval.

Table S10. List of primer sets used in the study

Gene	Species	Forward	Reverse
ATF4	Mouse	ATGGCCGGCTATGGATGAT	CGAAGTCAAACTCTTTCAGATCCATT
ATF6	Mouse	GGACGAGGTGGTGTCAGAG	GACAGCTCTTCGCTTTGGAC
CASP1	Mouse	TCCGCGGTTGAATCCTTTTCAGA	ACCACAATTGCTGTGTGTGCGCA
CASP3	Mouse	CCTCAGAGAGACATTCATGG	GCAGTAGTCGCCTCTGAAGA
CASP7	Mouse	GGACCGAGTGCCCACTTATC	TCGCTTTGTCGAAGTTCTTGTT
CASP9	Mouse	AGGAGGGACGAACACGTCT	CAAAGAAGGTTGCCCCAATCT
CHOP	Mouse	CTGCCTTTCACCTTGGAGAC	CGTTTCCTGGGGATGAGATA
FN1	Mouse	CGAGGTGACAGAGACCACAA	CTGGAGTCAAGCCAGACACA
GRP78	Mouse	GTCCTGCATCATCAGCGAAAG	GGTAGCCACATACTGAACACCA
GRP94	Mouse	GATGGTCTGGCAACATGGAG	CGCCTTGGTGTCTGGTAGAA
IL1β	Mouse	GCACTACAGGCTCCGAGATGAAC	TTGTCGTTGCTTGGTTCTCCTTGT
IL6	Mouse	GAGGATACCACTCCCAACAGACC	AAGTGCATCATCGTTGTTCATACA
IRE1α	Mouse	TGAAACACCCCTTCTTCTGG	CCTCCTTTTCTATTCGGTCACTT
PARP1	Mouse	GGAAAGGGATCTACTTTGCCG	TCGGGTCTCCCTGAGATGTG
PCSK9	Mouse	TGCAAAATCAAGGAGCATGGG	CAGGGAGCACATTGCATCC
PERK	Mouse	CCTTGGTTTCATCTAGCCTCA	ATCCAGGGAGGGGATGAT
PUMA	Mouse	TGTGGAGGAGGAGGAGTG	TGCTGCTCTTCTTGTCTCCG
sXBP1	Mouse	GAGTCCGCAGCAGGTG	GTGTCAGAGTCCATGGGA
TGFβ	Mouse	CAACAATTCCTGGCGTTACCTTGG	GAAAGCCCTGTATTCCGTCTCCTT
TNFα	Mouse	CATGAGCACAGAAAGCATGATCCG	AAGCAGGAATGAGAAGAGGCTGAG